

STATISTICS OF X-RAY POLARIZATION MEASUREMENTS

C. G. Montgomery¹

42 Blueberry Lane, Peterborough, NH 03458, USA

and

J. H. Swank²

Code 662, NASA Goddard Space Flight Center

Greenbelt, MD 20771, USA

`jean.swank@nasa.gov`

ABSTRACT

The polarization of an X-ray beam that produces electrons with velocity components perpendicular to the beam generates an azimuthal distribution of the ejected electrons. We present methods for simulating and for analyzing the angular dependence of electron detections which enable us to derive simple analytical expressions for useful statistical properties of observable data. The derivations are verified by simulations. While we confirm the results of previous work on this topic, we provide an extension needed for analytical treatment of the full range of possible polarization amplitudes.

Subject headings: methods: data analysis — method: statistical — polarization — X-rays: general

1. INTRODUCTION

X-ray polarimeters that are based on Compton scattering or the photoelectric effect lead to a distribution of events assigned to azimuthal angles in the plane perpendicular to the X-ray beam. The events are detected photons in the case of scattering experiments and detected electrons in

¹Professor of Physics and Astronomy (retired), University of Toledo, Toledo, OH, USA.

²Emeritus, X-Ray Astrophysics Laboratory

the experiments using the photoelectric effect. As in the case of polarization of optical and longer wavelengths, the polarization of the incoming radiation leads to a distribution

$$f(\phi) = I_f + U_f \cos(2\phi) + Q_f \sin(2\phi), \quad (1)$$

where I_f , U_f , and Q_f describe the distribution of electrons and should reflect the Stokes parameters of the incoming X-ray radiation. In general, detector characteristics and background cause the modulation of the signal to differ from that of the incoming beam. In this paper we address only the observed modulation. It would be that of the incoming beam for a perfect detector with negligible background.

Then the polarization amplitude and angle are

$$a_e = (U_f^2 + Q_f^2)^{1/2} / I_f \quad (2)$$

and the polarization angle estimate is

$$\phi_e = \frac{1}{2} \arctan(Q_f/U_f). \quad (3)$$

Recently the appropriate errors on the determination of X-ray polarization were discussed by Strohmayer & Kallman (2013, hereafter Paper 1), Elsner, O’Dell & Weisskopf (2012), Weisskopf, Elsner, & O’Dell (2010), and Weisskopf et al (2009). The best estimates and errors on the measurements of optical, infrared, and radio polarization have been discussed in a number of publications taking into account the techniques used for the measurements and their associated experimental errors (Vaillancourt 2006; Simmons & Stewart 1985; Clarke et al 1983; Wardle & Kronberg 1974; Serkowski 1962). While the polarization amplitude and angle are intuitively the focus of attention, they are not linearly related to the measurables and not independent. It has been pointed out that the Stokes U_f and Q_f are more amenable to statistical treatment. The same is true for X-ray polarization.

It has often been assumed that U_f/I_f and Q_f/I_f are independent, normally distributed variables. These then determine the probability of measured amplitude a_e and position angle ϕ_e , given the true amplitude a_0 and position angle ϕ_0 :

$$P(N, a_e, a_0, \phi_e, \phi_0) = \frac{Na_e}{4\pi} \exp\left[-\frac{N}{4}(a_e^2 + a_0^2 - 2a_e a_0 \cos 2(\phi_e - \phi_0))\right]. \quad (4)$$

Strohmayer & Kallman (2013) did extensive simulations for the range of polarization amplitudes 0 – 1. While there was agreement for small amplitudes, it was found that the simulation results differed as the amplitude approached 1.

We also carried out simulations, with a different approach, but also assuming Poisson errors on the number of events. We have kept the same convention for U_f and Q_f as used in Paper I, though other conventions are used, for example in radio astronomy (Hamaker & Bregman 1996). We likewise see divergence from Equation 4 for the joint probability in angle and amplitude. It is the purpose of this paper to point out that the divergence we find has a simple description that can be analytically derived. In Section 2 we describe our simulations and the analytical description. In Section 3 we ask what the confidence regions would be for the polarization, given a measurement. Section 4 summarizes the results.

2. GENERATION AND ANALYSIS OF SIMULATED DATA

We consider the case of measurements using the photoelectric effect. The partially polarized incident beam of X-rays can scatter electrons into various azimuthal angles around the axis of the incident beam. We want to estimate the degree of polarization in the incident beam, and its direction, from the observed numbers of electrons scattered into different azimuthal angles, and also the uncertainties in those estimates.

The polarized component of the beam scatters electrons into an azimuthal angle ϕ , measured from the direction of the incident polarization, with a probability proportional to $\cos^2(\phi)$, while the unpolarized component of the beam scatters electrons isotropically. In general, if the true polarization is at an angle ϕ_0 in a coordinate system, we would replace ϕ by $(\phi - \phi_0)$.

So we suppose that the number of scattered electrons reaching detectors, per unit time, at an azimuthal angle between ϕ and $(\phi + d\phi)$, can be expressed as proportional to $[I_0 + U_0 \cos(2\phi)]d\phi$.

This form ranges from $I_0 - U_0$ to $I_0 + U_0$ and has an amplitude of variation $a_0 = U_0/I_0$. a_0 is one of the physically significant quantities that we would like to estimate.

The detectors are taken to divide the interval from $-\pi$ to $+\pi$ into M equal angular bins, each of size $2\pi/M$ radians. M is an odd integer large compared with unity. The bins can be labelled with an index j which runs from $-(M-1)/2$ to $+(M-1)/2$, with the center of the j th bin at $\phi_j = 2\pi j/M$.

The expected number of counts in the j th bin in a time T is

$$\langle n_j \rangle = \frac{\kappa}{M} [I_0 + U_0 \cos(2\phi_j)] = \frac{\kappa I_0}{M} [1 + a_0 \cos(2\phi_j)]. \quad (5)$$

κ includes geometric and efficiency factors; it is proportional to T .

The values of n_j are independent Poisson-distributed random variables, with these mean values (and variances). The total number of counts

$$N = \sum_j n_j \quad (6)$$

is then Poisson-distributed with a mean (and variance) equal to

$$\langle N \rangle = \kappa I_0. \quad (7)$$

So a set of samples generated with the same $\langle N \rangle$ will have different total count numbers.

The mathematical properties of the n_j values enable deriving a number of useful facts about the statistical properties of various quantities related to them.

To estimate the incident polarization amount and direction from an observed set of n_j values, we seek to represent their angular distribution by a function describing the counts per unit angle.

$$f(\phi) = I_f + U_f \cos(2\phi) + Q_f \sin(2\phi). \quad (8)$$

Then the amount and direction of the incoming beam can be estimated in the usual way. For the amplitude of polarization the estimate is

$$a_e = (U_f^2 + Q_f^2)^{1/2} / I_f \quad (9)$$

and the polarization angle estimate is

$$\phi_e = \frac{1}{2} \arctan(Q_f/U_f). \quad (10)$$

The arctangent function in this equation is actually the two-argument arctangent function [represented in many programming languages as $\arctan 2(Q_f, U_f)$]. Technically, it is the principal value of the argument of the complex number $U_f + iQ_f$. Its values range from $-\pi$ to $+\pi$ radians, so ϕ_e ranges from -90° to $+90^\circ$.

Multiplying the function $f(\phi)$ by any constant produces no change in the amplitude and angle estimates.

There is a useful graphical representation of the results. To simplify the notation somewhat, let U' stand for U_f/I_f and Q' stand for Q_f/I_f . Then the amplitude and angle estimates are just given by

$$a_e = \sqrt{U'^2 + Q'^2} \quad (11)$$

and

$$\phi_e = \frac{1}{2} \arctan(Q'/U'). \quad (12)$$

If we think of U' and Q' as the rectangular coordinates of a point, these are the polar coordinates of that point: a_e is the distance of the point from the origin and $2\phi_e$ is the angle between the line from the origin to the point and the U' axis. It will be seen that it can be convenient to discuss the geometry of U' and Q' in the $U' - Q'$ plane and then, if desired, represent the results in plots of ϕ_e and a_e .

Choosing values of I_f , U_f , and Q_f that best represent the angular distribution of the set of n_j values could be done in several ways. If the amount of data is large enough, the results should be essentially the same. One approach would be to find the values that make the function f the best fit, in some sense, to the points. This was used in Paper 1, using chi-squared fitting.

Another approach, which is used here, is to view f as part of a discrete trigonometric interpolating polynomial, where the terms in the polynomial series are the ones that reflect the properties of the distribution that are of physical interest. We choose to express the angular distribution as

$$f(\phi_j) = \frac{M}{2\pi} n_j \quad (13)$$

Then I_f , U_f , and Q_f are the three coefficients that reflect the polarization of the incoming radiation and that enable estimates of its direction and amplitude.

The coefficients I_f , U_f , and Q_f are sums over the angles ϕ_j :

$$I_f = \frac{1}{2\pi} \sum_j n_j \quad (14)$$

$$U_f = \frac{1}{\pi} \sum_j n_j \cos(2\phi_j)$$

$$Q_f = \frac{1}{\pi} \sum_j n_j \sin(2\phi_j)$$

The coefficients I_f , U_f , and Q_f are random variables, the sums of linear combinations of the random n_j values. From the Lyapunov central limit theorem their distributions become normal as M becomes large enough, with means and variances which can be calculated using the sums over j of polynomials in $\cos(2\phi_j)$ and $\sin(2\phi_j)$. M does not appear in the limit. Our simulations were insensitive to M above 15.

The mean value of I_f is

$$\langle I_f \rangle = \frac{1}{2\pi} \sum_j \langle n_j \rangle = \kappa I_0 / (2\pi) = \langle N \rangle / (2\pi) \quad (15)$$

The other mean values are

$$\begin{aligned} \langle U_f \rangle &= \kappa U_0 / (2\pi) = \langle N \rangle a_0 / (2\pi) \\ \langle Q_f \rangle &= 0 \end{aligned} \quad (16)$$

The variance of I_f is

$$\text{Var}(I_f) = \frac{1}{4\pi^2} \sum_j \text{Var}(n_j) = \frac{1}{4\pi^2} \sum_j \langle n_j \rangle = \langle N \rangle / (4\pi^2) \quad (17)$$

and by similar calculations the variances of U_f and Q_f are each equal to

$$\sigma_f^2 = \kappa I_0 / (2\pi^2) = \langle N \rangle / (2\pi^2). \quad (18)$$

The covariance of Q_f with either I_f or U_f is zero, but the covariance of U_f with I_f is $\langle N \rangle a_0 / 4\pi^2$ and the correlation of U_f and I_f is $a_0 / \sqrt{2}$. Examples of correlation of U_f with I_f and Q_f with I_f were shown in Paper 1. For $\phi_0 \neq 0$, the correlation of Q_f with I_f is also nonzero.

The coefficients I_f , U_f , and Q_f are not statistically independent, since they are calculated from the same set of n_j values. In fact I_f , U_f , and Q_f are trivariate normal. This is not directly useful since the two quantities of interest are the ratios U_f/I_f and Q_f/I_f . Correct distributions for U' and Q' and thus for a_e and ϕ_e can be generated by simulations in which the M values of n_j are randomly generated for each sample, and the resulting values of I_f , U_f , Q_f and thus U' and Q' , can be used to get a_e and ϕ_e .

The points for a collection of samples will be centered around the U', Q' point with coordinates $a_0, 0$. Let us call that point Z . The probability density for points, that is, the probability per unit area in this plane, describes what fraction of the points from a set of many samples will have those locations. A line of constant probability, a closed curve enclosing the point Z , identifies the region within which a specific fraction of samples will lie, and thus the likelihood of that set of amplitude and angle estimates. Figure 1 shows an example for a low true amplitude.

Simplifications result if the variables U' and Q' are treated as if they were statistically independent random variables with known means and variances. In fact the available information allows a calculation of the marginal distribution of U' and Q' which shows that for large $\langle N \rangle$ they are independent. Details are given in Appendix A, which also provides the joint distribution of U' and Q' before any approximation of large $\langle N \rangle$.

The calculation also provides the means and variances of U' and Q' :

$$\langle U' \rangle = a_0 ; \quad \langle Q' \rangle = 0 ; \quad (19)$$

$$\text{Var}(U') = \frac{2}{\langle N \rangle} (1 - a_0^2/2) ; \quad \text{Var}(Q') = \frac{2}{\langle N \rangle}. \quad (20)$$

These results are confirmed by the results of simulations for the full range of amplitude values from 0 to 1.

The probability density for a system point would be the product of the probability density for U' and the probability density for Q' . But these are simply Gaussians with the derived variances and means. Figure 2 shows the results of simulations for a true polarization $a_0 = 3/4$, along with the Gaussian distributions with the calculated means and variances.

With the definition of λ as the ratio of the standard deviations:

$$\lambda^2 = \frac{\sigma_{Q'}^2}{\sigma_{U'}^2} = \frac{1}{1 - a_0^2/2} \quad (21)$$

and denoting $\sigma_{Q'}$ simply as σ' , the probability per unit area in the $U'Q'$ plane is also a Gaussian (see Equation(A.9)):

$$\begin{aligned} P_{U'Q'}(U', Q') &= \frac{\lambda}{2\pi\sigma'^2} \exp[-(U' - a_0)^2\lambda^2/2\sigma'^2] \cdot \exp(-Q'^2/2\sigma'^2) \\ &= \frac{\lambda}{2\pi\sigma'^2} \exp\left(-\frac{D^2}{2\sigma'^2}\right), \end{aligned} \quad (22)$$

with

$$D^2 = (U' - a_0)^2\lambda^2 + Q'^2. \quad (23)$$

It is worth noting that while these results were derived with the point Z on the U' axis (i.e., with $\phi_0 = 0$) they can be expressed in a way that is more general. Let us define 2η as the angular difference between the location of Z and the location of a data point. When Z is on the U' axis, η is just ϕ_e . But in general U' in the above equations is $a_e \cos(2\eta)$ while Q' is $a_e \sin(2\eta)$. Then Equation (23) becomes

$$D^2 = \frac{[a_e \cos(2\eta) - a_0]^2}{1 - a_0^2/2} + a_e^2 \sin^2(2\eta). \quad (24)$$

In this form it involves only the distances of Z and the data point from the origin and the angle between them, and is correct for any choice of a reference direction.

Lines of constant probability in the $U' - Q'$ plane are ellipses, centered on the point Z , with minor axes along the line from the origin to the point Z , and the ratio of major to minor axes equal to λ . An example is shown in Figure 3. D is the semi major axis of the ellipse. The area within an ellipse with a given D is $\pi D^2/\lambda$. The total probability of a point lying outside the ellipse with a given D is just $\exp(-D^2/2\sigma'^2)$ (as long as $D^2 \ll 1$.) See Figure 4 for an example of agreement between the probability distribution and a simulation.

This provides an extension of previous work, covering the full range of incident amplitudes, even when the correlation of I_f with U_f changes the variance of U' enough to be important. The results for U' and Q' also give

$$\text{Var}(a_e) = \sigma'^2(1 - a_0^2/2), \quad (25)$$

$$\text{Var}(\eta) = \frac{1}{4} \frac{\sigma'^2}{a_0^2}. \quad (26)$$

Since λ is quite close to unity unless the incident polarization amplitude is quite large, however, a simpler approximation should often be applicable. Setting $\lambda = 1$ reduces D^2 to

$$R^2 = (U' - a_0)^2 + Q'^2 \quad (27)$$

This is simply the square of the distance from the point with rectangular coordinates U' and Q' to the point Z . The probability density is

$$P_{U'Q'}(U', Q') = \frac{1}{2\pi\sigma'^2} \exp(-R^2/2\sigma'^2). \quad (28)$$

The lines of constant probability are simply circles centered at Z . The probability that a point is farther from Z than R is $\exp(-R^2/2\sigma'^2)$.

It is straightforward to reexpress this in terms of the polar coordinates a_e and $2\phi_e$, noting that the element of area in these coordinates is $a_e \cdot d(a_e) \cdot d(2\phi_e)$. Also, the variance $\sigma'^2 = 2/\langle N \rangle$ can be replaced by $2/N$ if the number of counts is large. The result is

$$P(a_e, \phi_e) = \frac{Na_e}{4\pi} \exp\left[-\frac{N}{4}(a_e^2 + a_0^2 - 2a_e a_0 \cos(2\phi_e))\right] \quad (29)$$

which is the formula commonly used in discussions of this topic (Weisskopf, Elsner, & O'Dell 2010; Strohmayer & Kallman 2013), the same as Equation(4) with $\phi_0 = 0$.

As pointed out by those authors, if the angle is not of interest, but only the amplitude of the polarization, the integral over angles gives the Rice distribution (Rice 1945) for the amplitude, a distribution used in various other signal processing applications. If, however, a_0 is not small and Equation (24) is applicable, the angular distribution is in the category of generalizations of the von Mises distribution (Mardia & Jupp 1999; Yfontis & Borgman 1982). It has been used in studies of Brownian motion, waves, and bending of biological molecules, for examples. The integral over angle gives a more complex distribution in a_e . This can certainly be numerically computed, if a

single parameter confidence region is desired. In this paper we are concentrating on joint confidence regions in the polarization amplitude and direction.

Comparison to the work of Strohmayer & Kallman (2013, Paper 1) finds some differences in the variances of U_f and Q_f and their correlations with I_f for the variables calculated in different ways. For a given simulation the results of calculating U_f and Q_f from trigonometric interpolating polynomials agree with the values obtained from unweighted least squares fitting (in accordance with Parseval’s theorem), but differ from the results of least squares weighted inversely with the counts in the bins (which exceeded 100 for all bins in our simulations). For the unweighted least squares, the variances of U_f and Q_f are independent of polarization and the correlations strictly linear, while for the weighted least squares, the variances decrease with amplitude. This in turn causes an amplitude dependent increase in the correlation magnitudes. It does not seem surprising that there is a difference in the distribution of the best fits and the shapes of the probability surfaces. The mean values of the fits are consistent.

Some details of our simulations and calculations are given in Appendix B.

3. DRAWING CONCLUSIONS FROM AN OBSERVED DATASET

We turn now to the question of how we can draw conclusions about the magnitude and direction of incoming X-rays from a single data set. We have the number of counts at each azimuthal angle with respect to some angle on the sky. We calculate I_f , U_f , and Q_f for our angular distribution of counts, and from them we compute two quantities: U' and Q' . We can think of these as the rectangular components of a point in a coordinate system with the U' axis in our reference direction. The origin of this coordinate system is the point corresponding to a completely unpolarized beam, for which both components would vanish.

What we do not know but would like to draw conclusions about is the location of the point Z in this coordinate system. By definition, Z is the point whose distance from the origin is the true polarization amplitude a_0 and which is in the same direction as the true polarization direction.

A contour line enclosing the observed data point can be defined by the fact that the probability of the observed U' and Q' values for any Z_C (the C stands for “candidate”) located at a point on that contour has the same value. Any point inside the contour is a location for Z_C that gives a probability of the data that is higher, and any point outside the contour is a location for Z_C such that the data has a lower probability. This defines a confidence region for Z_C .

We want to find the coordinates of the points Z_C for which the probability of the data point, with coordinates U' and Q' , has a specified probability. The geometry of this situation is very similar to the case previously studied, where one wanted to find which data points have a specified probability when the true amplitude is known. We define the angle $2\eta_C$ as the angle between lines from the origin to the data point and to Z_C , the difference between the angular position of the data point

and the angular position of the point Z_C .

In order to have a specified probability, the data point must lie somewhere on an ellipse whose center is at the point Z_C , whose major axis is perpendicular to the line from the origin to Z_C and has the length $2D$, and whose minor axis is $2D/\lambda_C$, with $\lambda_C = 1/\sqrt{1 - a_C^2/2}$. D is related to the probability in the same way as in the previous discussions; it depends only on the total number of counts in the data set and the specified probability.

From the earlier section, the requirement for the desired probability is given by Equation (24), which can be rewritten for the present purpose as

$$D^2 = \frac{[a_e \cos(2\eta_C) - a_C]^2}{1 - a_C^2/2} + a_e^2 \sin^2(2\eta_C). \quad (30)$$

We define a pair of new variables

$$u = a_C \cos(2\eta_C) ; \quad v = a_C \sin(2\eta_C) \quad (31)$$

which specify the location of Z_C relative to the data point. Using these, the condition that the data point have the correct position relative to Z_C can be written as

$$u^2(1 + D^2/2) - 2a_e u + v^2[1 + (D^2 - a_e^2)/2] = D^2 - a_e^2 \quad (32)$$

This is a quadratic in u and v and thus defines an ellipse. It is even in v , so the axes lie along and perpendicular to the line from the origin to the data point. The quadratic equation for u when $v = 0$ has two roots equidistant from $u = a_e/(1 + D^2/2)$, so the center of the ellipse is located at $u = a_e/(1 + D^2/2) ; v = 0$. The v semi-axis is $D/\sqrt{1 + D^2/2}$ and the u semi-axis is $[D/(1 + D^2/2)]\sqrt{1 + D^2/2 - a_e^2/2}$. (A more thorough and detailed derivation is provided in Appendix C.)

Since the derivation of probabilities in the earlier section included neglecting D^2 compared with unity, it is not inconsistent to do the same here. The result is simpler than might have been expected. The ellipse is centered on the data point and has axes of $2D$ and $2D/\lambda_e$. The data point and the candidate have changed places. Contour lines around the data point (in the $U'Q'$ plane) with a specified value of D are given by:

$$D^2 = (u - a_e)^2 \lambda_e^2 + v^2 \quad (33)$$

where $u = a_C \cos(2\eta)$ and $v = a_C \sin(2\eta)$ as defined in Equation (31), and 2η is the angle between the data point and the point on the contour.

One can then derive a description of probabilities similar to the situation of a known incident amplitude. The area of an ellipse with a given value of D would be just $\pi D^2/\lambda$, and the incremental area between ellipses for D and $D + dD$ would be proportional to DdD . An integral from D to infinity is then proportional to $\exp(-D^2/2\sigma'^2)$. Normalization makes the probability outside the contour equal to $\exp(-D^2/2\sigma'^2)$.

Figure 5 shows the implication of the results for a particular estimated polarization from a measurement sample. The marginal probability of U' and Q' derived in Section 1 is in terms of $\langle N \rangle$ for many samples. For a single sample, one has only the N for that sample. The probability depends on $\langle N \rangle D^2$ and is only significant for small D^2 . The fractional error in D^2 should be $1/\sqrt{N}$.

It seems likely that in any practical situation there will be large enough additional uncertainties in data acquisition not included in this statistical analysis that the difference in the contours for approximate or full inclusion of D^2 dependence would not be important.

It has been mentioned that statistical variations in the recorded counts result in a positive probability for any pair of U' and Q' values, even improbable ones which might lead to amplitude estimates that are larger than 1, while the true amplitude can only be zero or positive and less than or equal to 1. This could complicate the correct conclusions that can be drawn from a single data set if the total number of counts is too low or the confidence level chosen leads to a formal contour that extends into regions where $U'^2 + Q'^2$ is greater than 1. The simplest way to avoid such problems is just to get more data, or choose a different confidence level, or both, so that the contour is completely within the acceptable range. But if this is not feasible or desirable, one could impose restrictions and provide a truncated confidence region.

4. SUMMARY

The methods presented here for generating simulated counts of scattered electrons at different azimuthal angles, and for analyzing the resulting angular distribution, have the special advantage of making it possible to derive rigorous results about the estimation of polarization amplitudes and directions and their uncertainties. Alternative methods for generating simulations, and for analyzing the angular distribution, should give results that are essentially identical to these, but some of the predicted properties may only be observed rather than derived.

We confirm previous work on amplitude and angle estimates for cases in which the incident amplitude is not too large. With our approach we are able to provide analytical treatment for larger incident amplitudes, so that the entire physical range of possibilities is covered.

We thank Tod Strohmayer, Tim Kallman, and Phil Kaaret for detailed discussions.

A. THE DISTRIBUTIONS OF U_f, Q_f AND OF U', Q'

It is useful to introduce another variable, linear in U_f and I_f . Because $\langle U_f \rangle = a_0 \langle I_f \rangle$, the mean value of $(U_f - a_0 I_f)$ is zero and because the covariance of I_f with U_f is just a_0 times the variance of I_f , the covariance of $(U_f - a_0 I_f)$ with I_f is zero. The variance of $(U_f - a_0 I_f)$ is $\sigma_f^2(1 - a_0^2/2)$. We introduce the quantity

$$\lambda = 1/\sqrt{1 - a_0^2/2} \quad (\text{A.1})$$

and define the new variable

$$V_f = \lambda(U_f - a_0 I_f). \quad (\text{A.2})$$

V_f has a mean value of zero and the same variance as Q_f and is uncorrelated with I_f and Q_f .

The three variables, I_f , V_f , and Q_f are trivariate normal, and mutually uncorrelated, so they are independent. Then the joint probability distribution function is given by

$$P_{I,V,Q}(I_f, V_f, Q_f) = \frac{\sqrt{2}}{(2\pi\sigma_f^2)^{3/2}} \exp\left[-\frac{1}{2\sigma_f^2}(2(I_f - \langle I_f \rangle))^2 + V_f^2 + Q_f^2\right]. \quad (\text{A.3})$$

What we would like to have is the joint probability of $Q' = Q_f/I_f$ and $V' = V_f/I_f = \lambda(U' - a_0)$. To obtain this, we transform to V' and Q' as our variables, and integrate the probability of I_f, V', Q' over I_f . For the transformation we have $dV'dQ' = I_f^2 dV_f dQ_f$. Since V' and Q' only appear in the combination

$$D^2 = V'^2 + Q'^2 \quad (\text{A.4})$$

and $\langle I_f \rangle = \langle N \rangle / (2\pi) = \pi\sigma_f^2$, the integral to be evaluated is

$$P_{V'Q'}(V', Q') = \frac{\sqrt{2}}{(2\pi\sigma_f^2)^{3/2}} \int_{-\infty}^{\infty} dI_f I_f^2 \exp\left[-\frac{I_f^2}{\sigma_f^2}(1 + D^2/2) + 2\pi I_f - \pi^2 \sigma_f^2\right], \quad (\text{A.5})$$

which can be evaluated exactly. It is convenient to introduce

$$\sigma'^2 = \frac{1}{\pi^2 \sigma_f^2} = \frac{2}{\langle N \rangle} \quad (\text{A.6})$$

. Then

$$P_{V'Q'}(V', Q') = \frac{1 + (1 + D^2/2)/\langle N \rangle}{(1 + D^2/2)^{5/2}} \frac{1}{2\pi\sigma'^2} \exp\left(-\frac{D^2}{2\sigma'^2}\right). \quad (\text{A.7})$$

In any practical application, the value of $\langle N \rangle$ will be so large that the term proportional to $1/\langle N \rangle$ can be neglected in comparison with unity. Moreover, the values of D that might be of interest will be small enough to justify replacing $(1 + D^2/2)$ with unity. Otherwise, the probabilities involved are so small that they would be of no value. Accordingly the initial fraction in Equation(A.7) can be dropped, leaving

$$P_{V'Q'}(V', Q') = \frac{1}{2\pi\sigma'^2} \exp\left(-\frac{D^2}{2\sigma'^2}\right). \quad (\text{A.8})$$

The distribution of D^2 is just a chi-squared distribution with two degrees of freedom.

Thus it is clear that

$$P_{U'Q'}(U', Q') = \frac{\lambda}{2\pi\sigma'^2} \exp\left(-\frac{D^2}{2\sigma'^2}\right). \quad (\text{A.9})$$

This is the form in which U' and Q' are approximately independent normal variables with the variance in U' lower than that of Q' by $1 - a_0^2/2$. These results for the variance of U' and Q' agree with the estimates given by considering $\langle \delta^2 U' \rangle$ and $\langle \delta^2 Q' \rangle$, where expanding around the mean values gives $\delta U' = \delta U_f / \langle I_f \rangle - \langle U_f \rangle \delta I_f / \langle I_f \rangle^2$ and similarly for $\delta Q'$.

If $\phi_0 \neq 0$, the following means and covariances have a ϕ_0 dependence:

$$\begin{aligned} \langle U_f \rangle &= \frac{\langle N \rangle}{2\pi} a_0 \cos(2\phi_0), \\ \langle Q_f \rangle &= \frac{\langle N \rangle}{2\pi} a_0 \sin(2\phi_0), \\ \langle \delta U_f \delta I_f \rangle &= \frac{\langle N \rangle}{4\pi^2} a_0 \cos(2\phi_0), \\ \langle \delta Q_f \delta I_f \rangle &= \frac{\langle N \rangle}{4\pi^2} a_0 \sin(2\phi_0). \end{aligned} \quad (\text{A.10})$$

It remains true that

$$\langle \delta U_f \delta Q_f \rangle = 0.$$

With

$$\begin{aligned} X &= U \cos(2\phi_0) + Q \sin(2\phi_0), \\ Y &= -U \sin(2\phi_0) + Q \cos(2\phi_0), \\ Z &= \lambda(X - a_0 I_f), \end{aligned} \quad (\text{A.11})$$

corresponding to Equation (A.3), we have

$$P_{I_Z Y}(I_f, Z_f, Y_f) = \frac{\sqrt{2}}{(2\pi\sigma_f^2)^{3/2}} \exp\left[-\frac{1}{2\sigma_f^2} (2(I_f - \langle I_f \rangle))^2 + Z_f^2 + Y_f^2\right]. \quad (\text{A.12})$$

X, Y are just a set of axes rotated from U, Q by $2\phi_0$. Since

$$\begin{aligned} U &= a_e \cos(2\phi_e) \\ Q &= a_e \sin(2\phi_e), \end{aligned}$$

we have

$$\begin{aligned} X &= a_e \cos(2(\phi_e - \phi_0)) \\ Y &= a_e \sin(2(\phi_e - \phi_0)). \end{aligned}$$

The probability only depends on the angle between \mathbf{a}_e and the true polarization \mathbf{a}_0 , which is $2\eta = 2(\phi_e - \phi_0)$.

With $X' = X/I'$, $Y' = Y/I'$, and $D^2 = \lambda^2(X' - a_0)^2 + Y'^2$ the general result is derived as before, and similarly, for large $\langle N \rangle$,

$$P_{X'Y'}(X', Y') \approx \frac{\lambda}{2\pi\sigma'^2} \exp\left(-\frac{D^2}{2\sigma'^2}\right). \quad (\text{A.13})$$

B. COMPUTATIONAL REMARKS

Numerical implementation of the methods presented here for generating and analyzing simulations was done primarily with a simple Fortran program (available from the authors,) which can produce results for thousands of samples with thousands of counts each, in a few seconds on modest hardware.

Other simulations were done using IDL with version 8.2 RANDOMU to generate Poisson variates, both for n_j directly for 40 bins and for N in order to use the transformation method used by Strohmayer & Kallman (2013, Paper 1). To generate the n_j in this case the method of Marsaglia was used (Zelin & Severo 1964). These simulations were carried out to establish that the difference between the U and Q variances was due to the difference between the unweighted and weighted least-squares fits. The fits were carried out using IDL and the fitting routines based on MINPACK-1 (Markwardt 2009).

The locus of points a_e and η that satisfy Equation (24) can be obtained parametrically. Defining ρ by

$$\mathbf{a}_e = \mathbf{a}_0 + \rho \quad (\text{B.1})$$

and β as the angle between ρ and \mathbf{a}_0 , $a_e \cos(2\chi) = a_0 + \rho \cos(\beta)$ and $a_e \sin(2\chi) = \rho \sin(\beta)$. Then Equation (24) gives $\rho = D/\sqrt{\sin(\beta^2) + \cos(\beta^2)/(1 - a_0^2/2)}$ for $0 \leq \beta \leq 2\pi$. We then calculate

$$\begin{aligned} a_e^2 &= a_0^2 + \rho^2 + 2a_0\rho \cos(\beta), & (\text{B.2}) \\ \cos(2\chi) &= \frac{(a_0 + \rho \cos(\beta))}{a_e}, \\ \sin(2\chi) &= \frac{\rho \sin(\beta)}{a_e}, \\ 2\chi &= \arctan 2(\cos(2\chi), \sin(2\chi)). \end{aligned}$$

A similar parametric construction gives the contours of candidate true values of amplitude and angle, given measured values, as discussed in Section 3.

C. DERIVATION OF CANDIDATE CONTOURS

The probability of a particular measured polarization, given a known true polarization, depends only on D^2 (Equation (24) in the text), where

$$D^2 = \frac{[a_e \cos(2\eta) - a_0]^2}{1 - a_0^2/2} + a_e^2 \sin^2(2\eta). \quad (\text{C.1})$$

We wish to determine the candidate true polarizations a_C at angle 2η from a measured polarization amplitude and direction that would have a particular probability. The values must obey the same equation with $a_0 \rightarrow a_C$. The candidate point Z_C has the projections $u = a_C \cos 2\eta$ and $v = a_C \sin 2\eta$ parallel and perpendicular to \mathbf{a}_e . Then, using these substitutions and $a_C^2 = u^2 + v^2$, Equation (32) in the text is obtained, which can be written as

$$D^2 - a_e^2 - (u^2 + v^2)(1 + D^2/2) + a_e^2 \frac{v^2}{2} + 2a_e u = 0. \quad (\text{C.2})$$

The following sequence of reorganizations:

$$\frac{(D^2 - a_e^2)}{1 + D^2/2} - u^2 - v^2 + \frac{a_e^2 v^2/2}{1 + D^2/2} + \frac{2a_e u}{1 + D^2/2} = 0, \quad (\text{C.3})$$

$$\frac{(D^2 - a_e^2)}{1 + D^2/2} - \left(u - \frac{a_e}{1 + D^2/2}\right)^2 + \frac{a_e^2}{(1 + D^2/2)^2} - v^2 \left(1 - \frac{a_e^2/2}{1 + D^2/2}\right) = 0, \quad (\text{C.4})$$

$$\frac{D^2}{1 + D^2/2} - \frac{a_e^2}{1 + D^2/2} \left(1 - \frac{1}{1 + D^2/2}\right) - \left(u - \frac{a_e}{1 + D^2/2}\right)^2 - v^2 \left(1 - \frac{a_e^2/2}{1 + D^2/2}\right) = 0, \quad (\text{C.5})$$

$$\frac{D^2}{1 + D^2/2} \left(1 - \frac{a_e^2/2}{1 + D^2/2}\right) - \left(u - \frac{a_e}{1 + D^2/2}\right)^2 - v^2 \left(1 - \frac{a_e^2/2}{1 + D^2/2}\right) = 0. \quad (\text{C.6})$$

leads to

$$\frac{D^2}{1 + D^2/2} = \left(u - \frac{a_e}{1 + D^2/2}\right)^2 / \left(1 - \frac{a_e^2/2}{1 + D^2/2}\right) + v^2. \quad (\text{C.7})$$

This is the ellipse centered on $a_e/(1 + D^2/2), 0$ with semi-axes $(D/(1 + D^2/2))\sqrt{1 - a_e^2/2 + D^2/2}$ and $D/\sqrt{1 + D^2/2}$ for u and v , respectively. Now neglecting $D^2/2$ compared to 1,

$$D^2 = \frac{(u - a_e)^2}{1 - a_e^2/2} + v^2. \quad (\text{C.8})$$

REFERENCES

- Clarke, D., Stewart, B. G., Schwarz, H. E., & Brooks, A. 1983, A&A, 126, 260
 Elsner, R. F., O’Dell, S. L., & Weisskopf, M. C. 2012, Proc. SPIE, 8443, 84434N, astro-ph/1208.0610

- Hamaker, J. P., & Bregman, J. D. 1996, *A&AS*, 118, 161
- Mardia, K. V., & Jupp, P. E. 1999, *Directional Statistics* (New York: Wiley), 45
- Markwardt, C.B. 2009, in *ASP Conf. Ser. 411, Astronomical Data Analysis Software and Systems XVIII*, ed. D.A. Bohlender, D. Durand, & P. Dowler (San Francisco, CA:ASP), 251, [astro-ph/0902.2850](#)
- Rice, S.O. 1945, *Bell System Tech. J.*, 24, 46
- Serkowski, K. 1962, *AdA&A*, 1, 289
- Simmons, J. F. L., & Stewart, B. G. 1985, *A&A*, 142, 100
- Strohmer, T. E., & Kallman, T. R. 2013, *ApJ*, 773, 103 (Paper I), [astro-ph/1306.3885](#)
- Vaillancourt, J. E. 2006, *PASP*, 118, 1340, [astro-ph/0603010](#)
- Wardle, J. F. C., & Kronberg, P. P. 1974, *ApJ*, 194, 249
- Weisskopf, M. C., Elsner, R. F., Kaspi, V. M., et al. 2009, in *Neutron Stars and Pulsars (Astrophysics and Space Science Library, Vol. 357; berlin: Springer)*, 589
- Weisskopf, M. C., Elsner, R. F., & O’Dell, S. L. 2010, *Proc. SPIE*, 7732, 11, [astro-ph/1006.3711](#)
- Yfontis, E. A., & Borgman, L. E. 1982, *CoSTM*, 11, 1695
- Zelen, M. & Severo, N. C. 1964, in *Handbook of Mathematical Functions*, ed. M. Abramowitz & I. A. Stegun (Washington, DC: Government Printing Office), 925

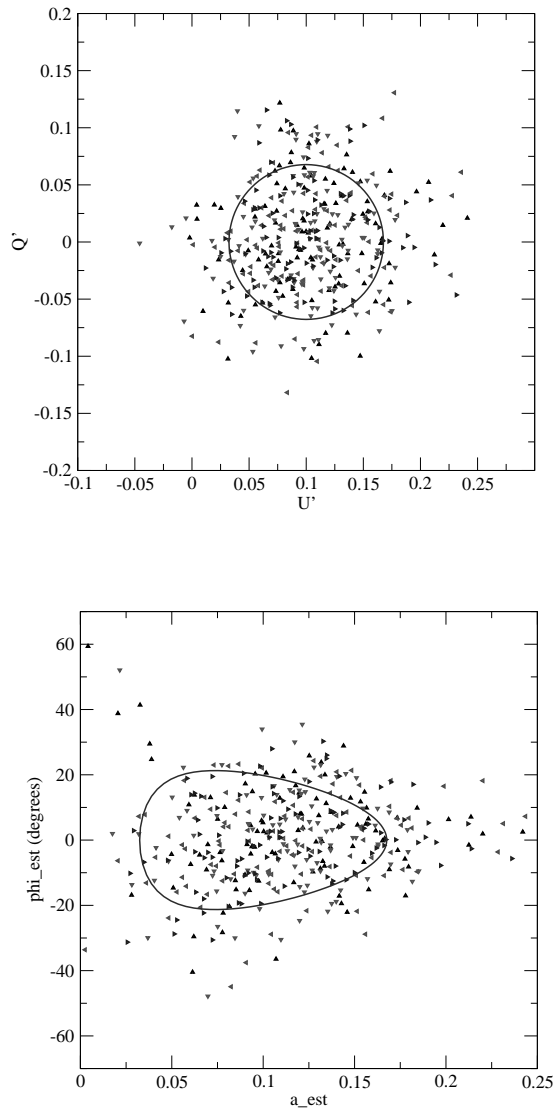


Fig. 1.— (top) U' and Q' for 4 sets of 100 simulations each for $\langle N \rangle = 1000$, with the true polarization along the U_f axis. Points from the different sets are indicated by triangles of different orientation. The 68.3 % probability contour is centered on the point Z at $a_0 = 0.1, 0$. (bottom) The polarization amplitude a_e and angle ϕ_e corresponding to the U' and Q' results. ϕ_e is half the angle between the U' axis and the direction to the point U', Q' .

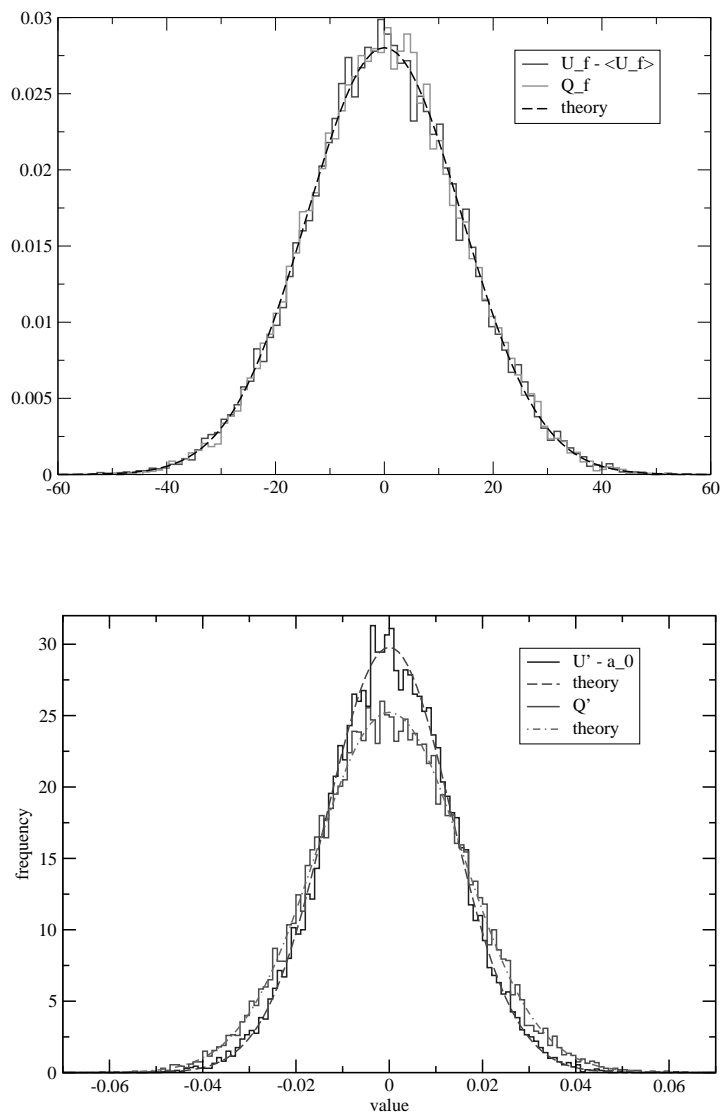


Fig. 2.— (top) Marginal distributions of U_f and Q_f for 20,000 simulations with $\langle N \rangle = 4000$ for a polarization $a_0 = 3/4$ along the U_f axis. The theoretical distributions are the same. (bottom) Marginal distributions of U' and Q' for 20,000 simulations with $\langle N \rangle = 8000$ for a polarization $a_0 = 3/4$ along the U_f axis. Here the ordinate is the number of simulations in a bin. The curves are the predictions for independent normal distributions.

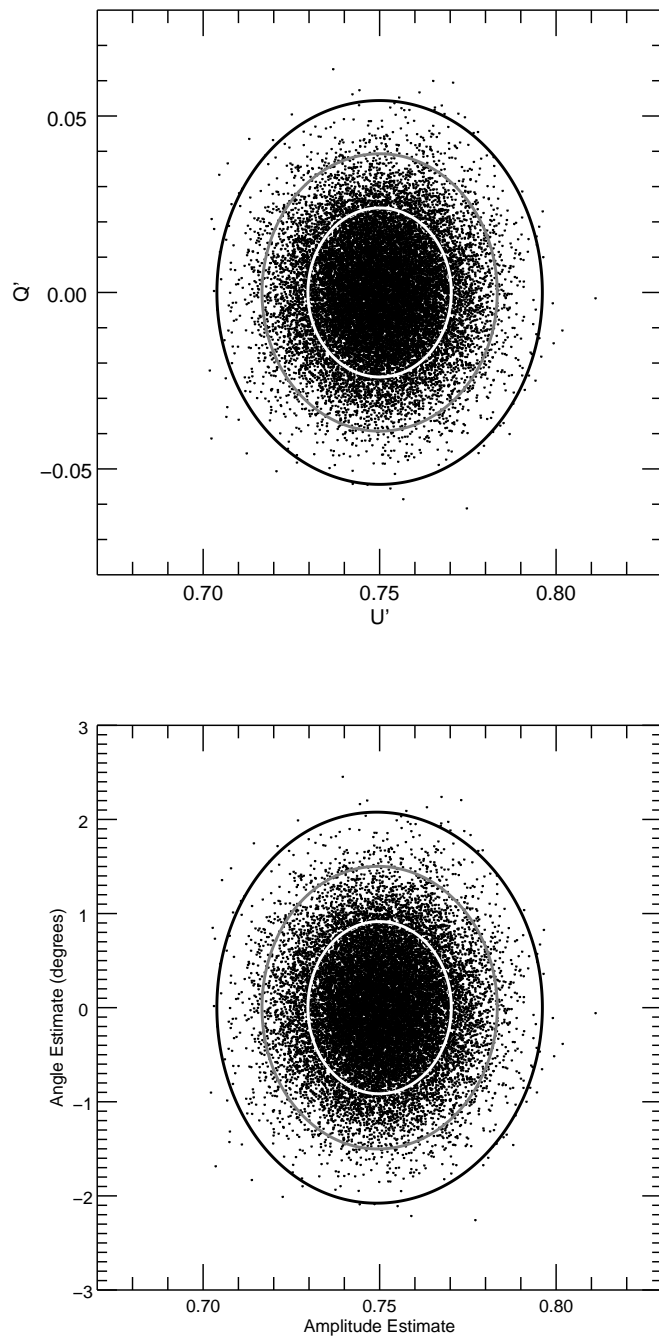


Fig. 3.— (top) Distribution of U' and Q' for 20,000 simulations (the same as for Fig 2, bottom) with $\langle N \rangle = 8000$, $a_0 = 3/4$, and $\phi_0 = 0$. Contours of the predicted 1, 2, and 3 sigma levels (68.27, 95.45, and 99.73 %) are superposed. 13597, 19010, and 19935 simulations fell within those contours, in comparison to 13654, 19090, and 19946 expected. The semi-major axes are along the Q' axis and the semi-minor axes along the U' axis, centered on $a_0, 0$. (bottom) The corresponding a_e and ϕ_e with their theoretical contours.

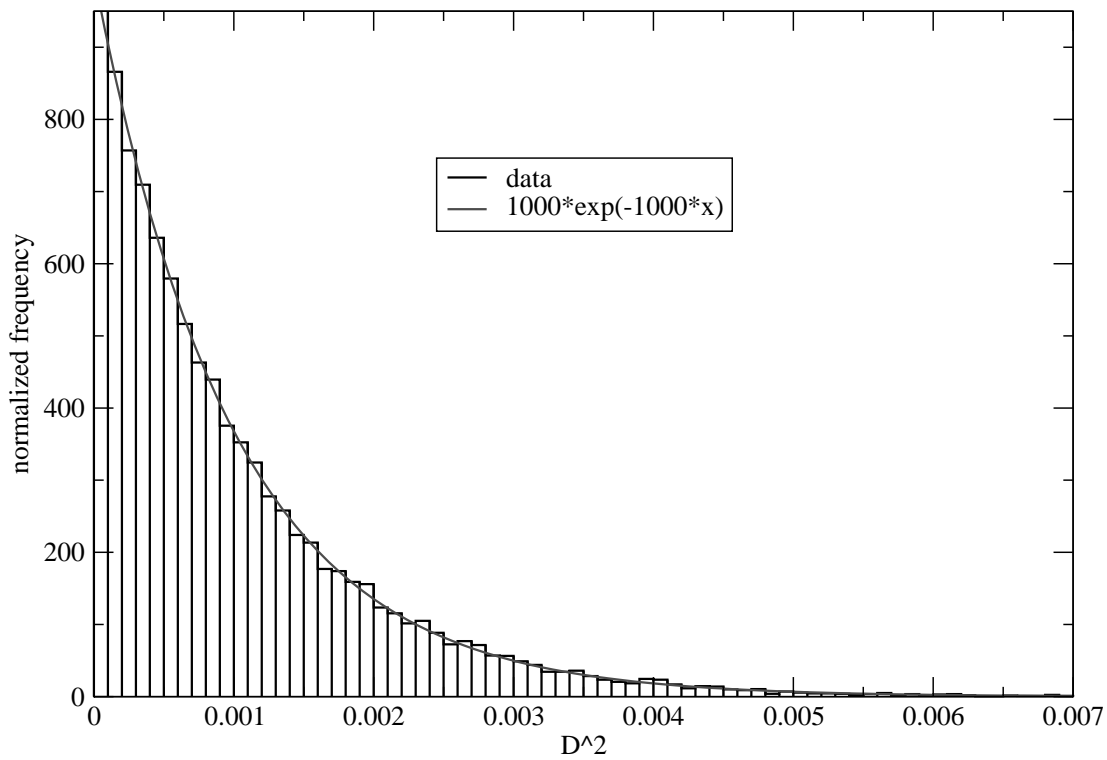


Fig. 4.— Distribution in D^2 for a simulation with $a_0 = 3/4$ and $\langle N \rangle = 4000$, for $N_{sample} = 20,000$. The number of samples in a D^2 increment $\Delta D^2 = 10^{-4}$, is plotted, normalized by $N_{sample}\Delta D^2 (= 2)$, together with the expected values. For this case $1/2\sigma'^2 = 1000$. The probability for the measured polarization to lie outside of D^2 matches the predicted exponential.

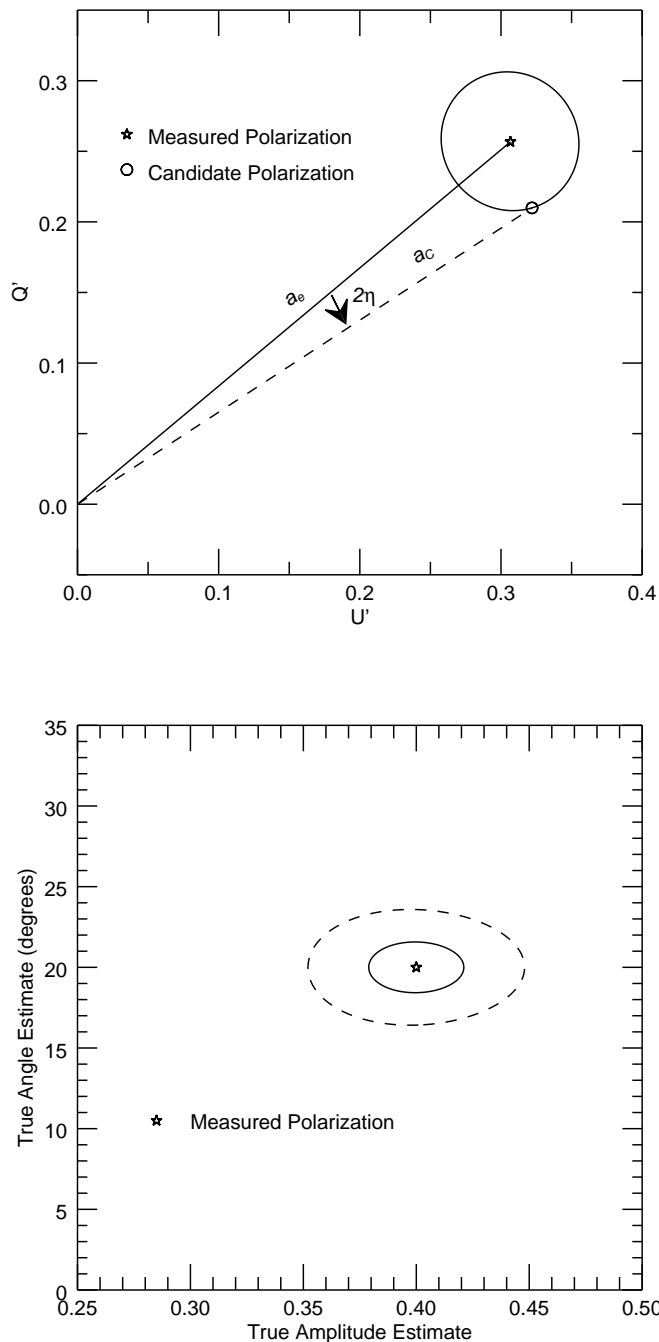


Fig. 5.— Examples of contours for the candidate true polarization quantities for a measurement of $a_e = 0.40$ and $\phi_e = 20$ degrees. (top) Contour for 68.3 % (theoretical) confidence in $U'Q'$ space for the true polarization, for $D = 0.05$. The dashed line indicates a candidate true polarization at distance a_C from the origin and angle 2η from the measured polarization. (bottom) Contours (solid and dashed lines, respectively) of 1 sigma (68.3 %) and 3 sigma (99.7 %) for the true amplitude and angle, for $N = 9500$ events.